Acta Oceanol. Sin., 2025, Vol. 44, No. 3, P. 161–171
https://doi.org/10.1007/s13131-025-2464-6

Simulation and analysis of the snow blowing on landfast sea ice, Antarctica

Guanghua Hao[1], Hui Shen[1], Yongming Sun[2*]

[1] Key Laboratory of Marine Hazards Forecasting, National Marine Environmental Forecasting Center, Ministry of Natural Resources, Beijing 100081, China

[2] College of Oceanic and Atmospheric Sciences, Ocean University of China, Qingdao 266100, China

Received 1 July 2024; accepted 8 October 2024

© Chinese Society for Oceanography and Springer-Verlag GmbH Germany, part of Springer Nature 2025

Abstract

Sea ice and snow are the most sensitive and important crucial components of the global climate system, affecting the global climate by modulating the energy exchange between the ocean and the atmosphere. The sea near Zhongshan Station in Antarctica is covered by landfast sea ice, with snow depth influenced by both thermal factors and wind. This region frequently experiences katabatic winds and cyclones from the westerlies, leading to frequent snow blowing events that redistribute the snow and affects its depth, subsequently impacting the thermodynamic growth of sea ice. This study utilized the one-dimensional thermodynamic model ICEPACK to simulate landfast sea ice thickness and snow depth near Zhongshan Station in 2016. Two parameterization schemes for snow blowing, the Bulk scheme, and the ITDrdg (ITD/ridges) scheme are evaluated for their impact on snow depth. The results show that simulations using snow blowing schemes more closely align with observed results, with the ITDrdg scheme providing more accurate simulations, evidenced by root mean square errors of less than 10 cm for both snow depth and sea ice thickness. Snow blowing also impacts the thermodynamic growth of sea ice, particularly bottom growth. The sea ice bottom increases by 9.0 cm using the ITDrdg scheme compared to simulations without the snow blowing, accounting for 12.5% of total sea ice bottom growth. Furthermore, snow blowing process also influences snow ice formation, highlighting its primary role in affecting snow depth. Continued field observations of snow blowing are necessary to evaluate and improve parameterization schemes.

Key words landfast sea ice, snow blowing, sea ice thickness, Prydz Bay Antarctic, sea ice thermodynamic growth

Citation Hao Guanghua, Shen Hui, Sun Yongming. 2025. Simulation and analysis of the snow blowing on landfast sea ice, Antarctica. Acta Oceanologica Sinica, 44(3): 161–171, doi: 10.1007/s13131-025-2464-6

1 Introduction

Sea ice and snow are important components of the global climate system, playing a crucial role in reflecting a large portion of incoming solar radiation. Antarctic sea ice has exhibited a stable and gradual increasing trend since the beginning of satellite observations (Parkinson, 2019). The variability of Antarctic sea ice is influenced by multiple factors and exhibits distinct regional characteristics. Declines in Antarctic sea ice have primarily been observed in the Weddell Sea and the Ross Sea (Parkinson, 2019; Hao et al., 2021b), though these long-term changes are not statistically significant. Currently, it remains unclear whether the decrease in Antarctic sea ice since 2014 was the initiation of a long-term decline trend (Hobbs et al., 2016). As a cooling source for the Earth, Antarctica has a profound impact on global climate change, with sea ice being an essential component of the Antarctic climate system. Therefore, it is essential to strengthen observational and simulation research on Antarctic sea ice.

Zhongshan Station, located in Prydz Bay, Southeast Antarctica, is surrounded by landfast sea ice, which remains stationary relative to the land but experiences vertical movement due to tidal influences. The presence of landfast sea ice significantly affects China's scientific exploration and logistical support at Zhongshan Station. Monitoring sea ice in Antarctica is of great significance. However, substantial errors exist in satellite-derived sea

Foundation item: The National Natural Science Foundation of China under contract Nos 42306255 and 41976217; the National Key R&D Program of China under contract No. 2018YFA0605903.
*Corresponding author, E-mail: sym@ouc.edu.cn

ice thickness due to limitations in resolution and issues such as cloud cover in satellite remote sensing data. The accuracy of satellite-derived sea ice thickness is also affected by snow on the ice surface, which can alter the albedo of sea ice (Willatt et al., 2010; Kwok and Kacimi, 2018). Long-term continuous observations of landfast sea ice thickness are scarce, relying mainly on limited manual observations and sea ice temperature buoy observations. Consequently, reliable data on Antarctic sea ice thickness variations, particularly for nearshore landfast sea ice, remain inadequate. As a result, numerical simulation has become an important tool for studying Antarctic sea ice, especially nearshore landfast sea ice.

Snow blowing commonly occurs on the surface of sea ice (Trujillo et al., 2016), redistributing snow and affecting its depth. The process of snow blowing changes the distribution of snow over time and space (Vionnet er al., 2014), leading to inconsistent snow distribution due to topographic influences (Durand et al., 2005; Mott et al., 2010). Landfast sea ice near Zhongshan Station is affected by katabatic winds (Xie et al., 2002； Sun et al., 2016) and cyclones from the edge of the westerlies, which bring strong winds during snowfall events. Consequently, snow blowing frequently occurs on the landfast sea ice near Zhongshan Station, significantly affecting snow depth.

Sea ice growth is influenced by the thermodynamic energy balance. Sea ice and its snow cover act as an insulating layer between the atmosphere and the ocean, affecting the thermodynamic growth and mass balance of the sea ice (Trujillo et al., 2016). Snow has a high albedo, reducing incoming shortwave radiation. The presence of snow on the ice surface further affects the energy exchange in the atmosphere-ice-ocean in polar regions. In Antarctica, thick snow cover limits the thermodynamic growth of sea ice (Powell et al., 2005; Lewis et al., 2011). Excessive snow depth can lead to negative freeboard thickness of sea ice, resulting in the formation of snow ice as snow is compacted by seawater (Leppäranta, 1983). During the melting season, the melting and refreezing of snow contribute to increased sea ice thickness (Cheng et al., 2003; Wang et al., 2015).

Changes in snow depth impact the absorption of solar radiation by landfast sea ice, altering its thermodynamic balance and affecting sea ice thickness simulations. This study uses the one-dimensional thermodynamic numerical model ICEPACK to simulate the influence of snow blowing on snow depth and thermodynamic growth on landfast sea ice, which experiences minimal horizontal movement and is primarily influenced by thermodynamic process. Two existing parameterization schemes for snow blowing in the ICEPACK model are employed, and the results are evaluated against *in-situ* observation data to quantitatively analyse the impact of different snow blowing parameterization schemes on snow accumulation and sea ice growth processes.

2 Data and method

2.1 *In-situ observations*

Observational data were collected from landfast sea ice near Zhongshan Station between April and November 2016 (Fig. 1a). The observation site was located on landfast sea ice, approximately 600 m north of Zhongshan Station (Fig. 1b) (Hao et al., 2019, 2021a). Both automatic weather station (AWS) measurements and manual observations were conducted at the site (69°22′S, 76°22′E). The AWS recorded hourly observations of wind speed, wind direction, air temperature, relative humidity, surface temperature, and solar radiation. Wind was measured using three-dimensional sonic anemometer (CSAT3B), while air temperature and relative humidity were recorded with an HMP155 sensor. Surface temperature was monitored using an SI-111 sensor, and solar radiation was measured

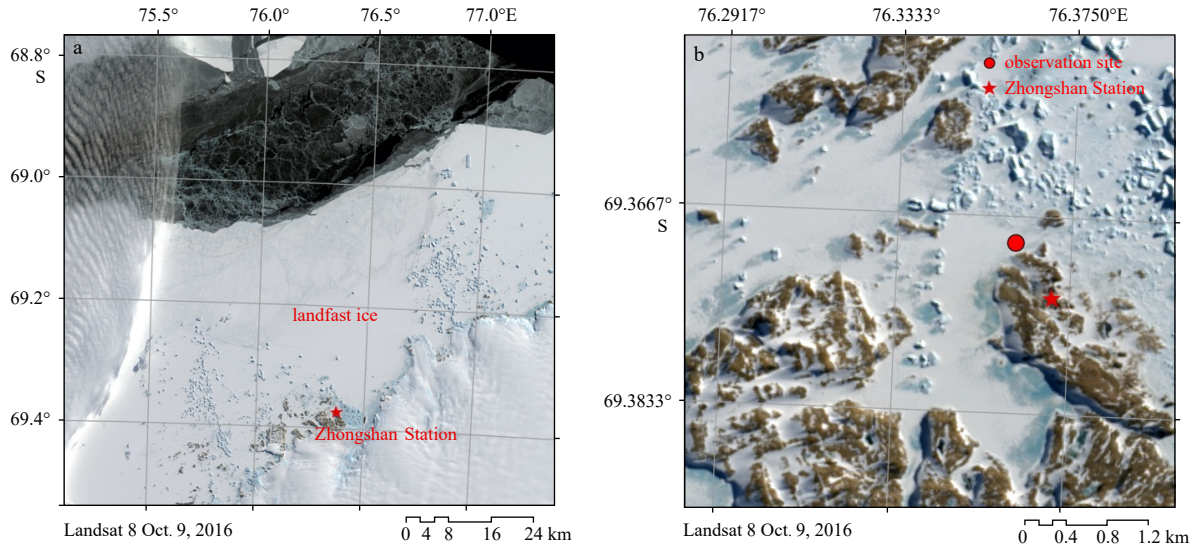


Fig. 1. Map of the location of Zhongshan Station (a) and the observation site on nearby landfast sea ice (b). The AWS were set up, and manual observations were carried out at the site.

using a Kipp & Zonen CNR4 sensor. Daily precipitation equivalent data were obtained from the Russian Progress II Station, measured using a Tretyakov's snow-rain pail located approximately 1.0 km from the AWS site, and were used for numerical simulations of atmospheric foßrcing (Hao et al., 2021a).

Sea ice temperature buoy and manual observations were also utilized. A sea ice temperature buoy, deployed approximately 200 m from the AWS, automatically recorded air-ice-sea temperature data. Developed by Taiyuan University of Technology, the buoy had a resolution of 0.062 5℃, an accuracy of 0.5℃, and a sensor spacing of 1.0 cm, with 250 sensors installed (Hao et al., 2019). The buoy's sea ice temperature data were used for comparison with simulated sea ice temperatures. Sea ice thickness was calculated based on temperature gradient differences in different media using buoy's sea ice temperature data (Hao et al., 2019), and these calculations were used to evaluate the simulated sea ice thickness. Manual observations included snow depth and drilled sea ice thickness data, conducted approximately once every seven days, depending on the weather, starting from April 22, 2016. Manual observations were conducted near the AWS site. Snow depth was manually measured using a ruler, and ice thickness was determined by drilling a hole at nearly the same location. The sea ice thickness data calculated from the buoy had an error of less than 7 cm compared to manually observed data (Hao et al., 2019).

2.2 *Weather conditions*

During the observation period, which covered the sea ice freezing season until the onset of melt, the air temperature exhibited a fluctuating pattern (Fig. 2a), averaging −15.5℃. Prior to October, air temperatures declined, reaching their lowest values in late June, early July, and early September. Starting in October, temperatures increased, surpassing 0℃ in early November. Zhongshan Station, located on the Larsemann Hills near the Amery Ice Shelf, has a slope of approximately 10–15 m/km towards the south and is influenced by local topography. The station experiences katabatic winds from the east, typically beginning in the evening and weakening by noon the following day. The northern part of Zhongshan Station is mostly covered by landfast sea ice (Fig. 1a). The local terrain results in stronger temperature differences between day and night and stronger katabatic winds from the ice sheet as weather clears. The average wind speed during the observation period was 4.2 m/s, with clear diurnal variations (Fig. 2b). After October, with rising temperatures, the day-night temperature differences increased, strengthening of the katabatic wind. The frequency of wind speeds exceeding 10 m/s also increased. Precipitation during the observation period primarily occurred as snowfall. Several significant snowfall events occurred in early July, early September, and late October (Fig. 2c). The most severe daily snowfall occurred in early July, significantly contributing to snow depth accumulation.

2.3 *Model introduction*

The ICEPACK model, a one-dimensional sea ice thermodynamic model, was used in this study. Released in 2018, it serves as the thermodynamic component of the global sea ice model CICE, developed by the Los Alamos National Laboratory in the USA. ICEPACK incorporates a comprehensive range of physical processes and complex parameterization schemes. Version 1.3.0 of ICEPACK includes advanced snow processes (Hunke et al., 2021), such as two snow blowing schemes: the Bulk snow redistribution scheme (Bulk) and the Snow redistribution and compaction by wind scheme (ITD/ridges, ITDrdg), both focusing on the impact of snow depth. In the Bulk scheme, snow blowing occurs by reducing snowfall reaching the ice surface, assuming the reduced snow enters the ice leads. The ITDrdg scheme considers snow-wind interactions, determining wind's effect on snow through densification (Lecomte et al., 2015).

In the Bulk scheme, a parameter p is defined as the ratio of snow on ridges to that on level ice. The snow blowing process reduces the snowfall reaching the ice surface, assuming the reduced snow is transported to the leads.

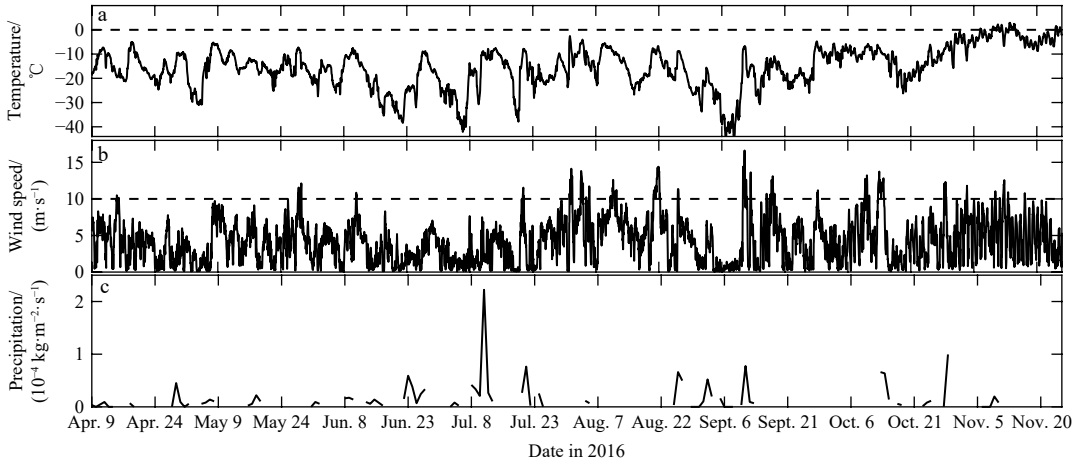


Fig. 2. Time series of hourly 2 m air temperature (a), wind speed (b), and daily cumulative snow precipitation (c) during April 9, 2016–November 22, 2016. The dash lines in a and b indicate 0℃ and 10 m/s, respectively.

Surface Heat Budget of the Arctic Ocean (SHBEA) observations indicate that snow near ridges is 30% thicker compared to that on level ice, with a default p of 0.3 (Sturm et al., 2002). In the ITDrdg scheme, the snow blowing process is achieved by controlling the interaction between wind speed and snow. The snow is compacted by the wind, and once the snow density reaches a certain value, it is no longer affected by snow blowing. The scheme's default maximum snow density is 450 kg/m^3. Both two snow blowing schemes, along with a no snow blowing scheme, were used in ICEPACK to quantitatively study the impact of snow blowing processes on snow depth and sea ice thermodynamic growth. Seven experiments were conducted: a control experiment (Ctrl) with no snow blowing scheme, Bulk scheme experiments with p values of 0.2, 0.3, and 0.4, and ITDrdg scheme experiments with maximum snow densities of 400 kg/m^3, 450 kg/m^3, and 500 kg/m^3 (Table 1).

The initial sea ice thickness and snow depth used in the simulations were based on observations from April 7, 2016, which recorded values of 85 cm and 10 cm, respectively. Atmospheric forcing used AWS observations and precipitation records from the Progress Ⅱ Station between April and November 2016. Oceanic forcing used ECMWF ORAS5 (Ocean ReAnalysis System 5) data (Zuo et al., 2019) and outputs from the Parallel Ocean Program model (POP) (Collins et al., 2006), including sea surface temperature, sea surface salinity, boundary layer depth, and zonal and meridional currents.

3 Results

Landfast sea ice near Zhongshan Station typically begins to freeze in late March or early April. It starts to break up in mid to late January of the following year, reaching its minimum extent by the end of February. Landfast sea ice begins to melt in November with rising air temperature, primarily due to bottom melting. Observations primarily focused on the freezing period of landfast sea ice for safety reasons, thus the simulations in this study mainly concentrated on the freezing period, including the initial melting phase.

3.1 *Snow simulation*

The simulated snow depth closely matched manual observations before July (Fig. 3a). A significant snowfall event on July 8 (Fig. 2c) led to a noticeable increase in snow depth. By July 13, the observed snow depth was

Table 1. Design of simulation experiments (Exp.) with different p values in the Bulk scheme and different densities in the ITDrdg scheme

	Ctrl	Exp. 1	Exp. 2	Exp. 3	Exp. 4	Exp. 5	Exp. 6
Scheme	none	Bulk	Bulk	Bulk	ITDrdg	ITDrdg	ITDrdg
p	–	0.2	0.3	0.4	–	–	–
Density/(kg·m^{-3})	–	–	–	–	400	450	500

Note: p represents the ratio of snow on ridges to snow on level ice, which is utilized in the Bulk scheme, while density signifies the maximum snow densities threshold employed in the ITDrdg scheme. − represents no value.

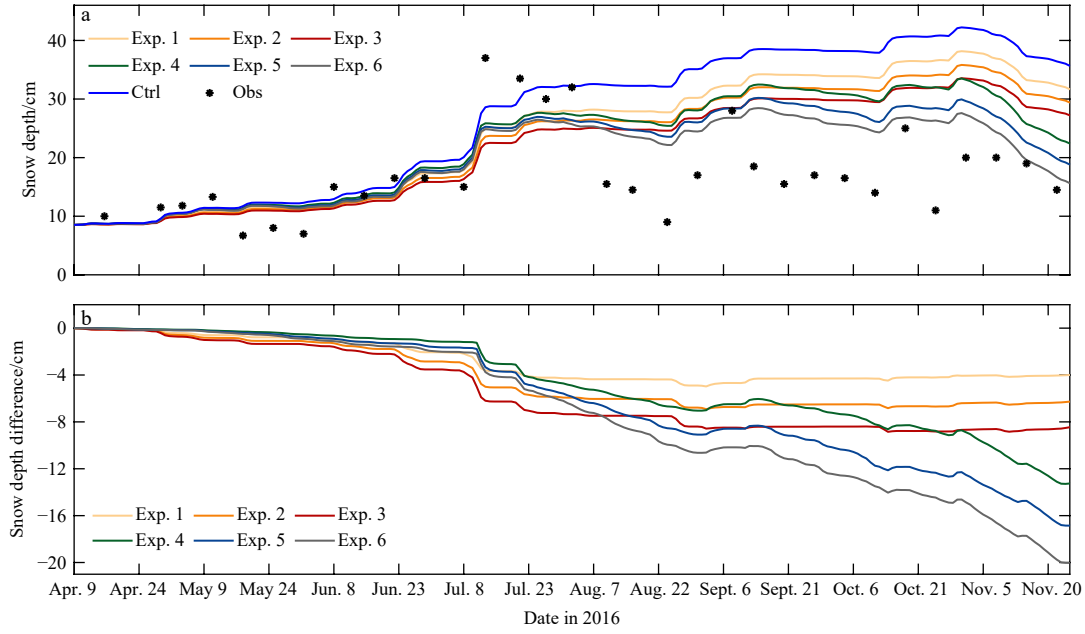


Fig. 3. Simulated snow depth using different snow blowing parameterization scheme and observed snow depth (a) and the snow depth difference between other experiments and the Crtl experiment (b). Obs means the manual observation of snow depth.

37.0 cm but began decreasing as the snowfall event ended.

In the Ctrl experiment, the simulated snow depth on July 13 was 28.6 cm. Using the Bulk parameterization scheme with different p values, the simulated snow depths were 25.0 cm, 23.6 cm, and 22.4 cm for Exps 1−3, respectively. With the ITDrdg scheme, the snow depths were 25.9 cm, 25.3 cm, and 24.8 cm for Exps 4−6. Compared to the Ctrl experiment, the Bulk scheme generally resulted in decreased snow depth except during snowfall events, where it remained constant or increased. As the p value increased and snowfall on the level ice surface decreased, the simulated snow depth decreased. In the ITDrdg scheme, snow depth increased during snowfall events and then gradually decreased. Both schemes simulated thinner snow depths compared to the Ctrl experiment. The difference in snow depth between the Bulk scheme and the Ctrl experiment remained relatively stable. However, in the ITDrdg scheme, this difference increased over time (Fig. 3b). This is because, in the Ctrl and Bulk experiments, snow depth was not affected by wind after snowfall. In contrast, in the ITDrdg scheme, the snow continued to be influenced by wind until the wind speed dropped below a certain threshold and the snow density reached its maximum threshold.

In the Ctrl experiment, snow depth accumulated during snowfall events and began to decrease after surface melting commenced in mid to late November. The Bulk scheme reduced snow accumulation by decreasing precipitation, while the ITDrdg scheme accounted for wind effects on snow, leading to a decrease in snow depth post-snowfall events. After November, snow depth in the ITDrdg scheme decreased significantly due to melting and wind effects. Higher maximum density settings in the ITDrdg scheme led to greater reductions in snow depth. The results indicated that the ITDrdg scheme simulated snow depths closer to manually observed values (Table 2), capturing the overall trend of snow depth changes, including the gradual decrease due to wind from July 13 to August 22, consistent with observed values.

3.2 *Sea ice simulation*

All experiments captured the general trend of sea ice variation, including a decrease in thickness due to melting after November (Fig. 4). Simulated sea ice thickness during April 9, 2016–December 25, 2016 was generally thinner compared to the manually observed and buoy cal-

Table 2. Bias and root mean square errors (RMSEs) between the simulated snow depth, sea ice thickness and sea ice temperature in different simulation experiments and the observed snow depth, buoys-based sea ice thickness and buoy-based sea ice temperature

Metric	Variable	Value						
		Ctrl	Exp. 1	Exp. 2	Exp. 3	Exp. 4	Exp. 5	Exp. 6
Bias	Snow depth/m	10.2	7.2	5.8	4.6	5.6	4.0	2.9
	Sea ice thickness/cm	−7.0	−5.5	−4.6	−3.8	−2.7	−1.8	−1.2
	Sea ice temperature/℃	0.2	−0.1	−0.2	−0.3	−0.3	−0.4	−0.5
RMSE	Snow depth/m	14.9	12.1	10.8	9.7	9.7	8.1	7.1
	Sea ice thickness/cm	12.5	11.4	10.6	9.9	9.5	8.8	8.2
	Sea ice temperature/℃	0.6	0.5	0.5	0.6	0.5	0.6	0.7

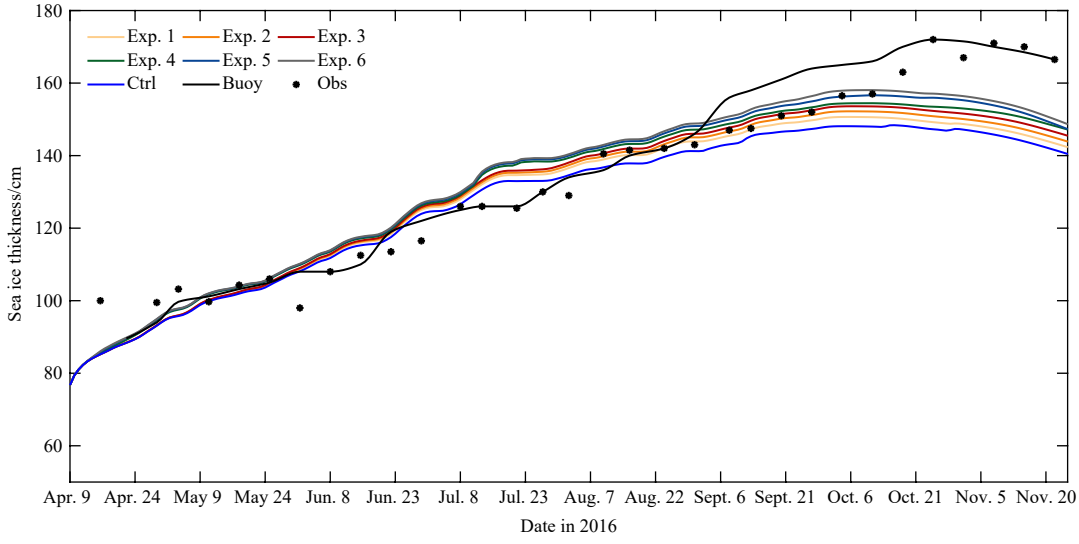


Fig. 4. Simulated sea ice thickness using different snow blowing parameterization scheme and observed sea ice thickness. Buoy means the temperature buoy calculated sea ice thickness and Obs means the manual observation of sea ice thickness.

culated thicknesses. The average buoy observed thickness during this period was 136.5 cm, while simulated averages were 127.1 cm, 128.6 cm, 129.4 cm, 130.1 cm, 131.2 cm, 132.1 cm, and 132.7 cm for the Ctrl experiment and Exps 1−6 experiments, respectively. The Ctrl experiment demonstrated the thickest snow depth but the thinnest sea ice thickness. Simulated and observed sea ice thicknesses are similar until July (Fig. 4). After July 8, significant differences in sea ice thickness emerged (Fig. 4), correlating with increased disparities in simulated snow depth (Fig. 3b). The differences in snow depth is significant and often corresponds to considerable difference in sea ice thickness (Table 2).

Simulated sea ice temperature corresponded well with changes observed by sea ice temperature buoys. The average simulated sea ice temperature was −6.0℃, −6.2℃, −6.4℃, −6.5℃, −6.5℃, −6.6℃, and −6.7℃ for Ctrl and Exps 1−6, while the observed average was −6.2℃. The Ctrl experiment showed a slightly higher average temperature than observed. Before July 13, the average simulated temperature was −7.3℃, slightly lower than the observed −7.2℃. The average temperatures of other experiments were lower than −7.3℃. After July 13, the average observed temperature was −5.6℃, while simulated averages were −5.1℃, −5.4℃, −5.6℃, −5.7℃, −5.7℃, −5.8℃, and −5.9℃ for Ctrl and Exps 1−6. The Ctrl and Exp. 1 simulations showed higher average temperatures than observed (Table 2), consistent with the snow depth simulation results. The thickest snow depth in the Ctrl experiment effectively isolated energy exchange between the ice and atmosphere.

Simulated sea ice thickness and temperature were influenced by snow depth. During the initial stage (before July 8), minimal snowfall resulted in negligible differences in snow depth (Fig. 3b), sea ice thickness (Fig. 4), and sea ice temperature (Fig. 5) among different experiments, closely matching observed results. As snow depth accumulated, differences in simulated snow depth, sea ice thickness, and sea ice temperature between the Ctrl experiment and other parameterization schemes increased, with simulated values generally higher than observed (Fig. 3a).

During the second stage (after July 8), thicker snow depth in the Ctrl experiment acted as an insulator, resulting in higher sea ice temperatures and influencing ice growth. The ITDrdg scheme simulated lower average sea ice temperatures than observed. The maximum simulated sea ice thicknesses (154.5 cm, 156.6 cm, and 158.1 cm) were smaller than manual observations and buoy calculations (172.0 cm). The ITDrdg scheme's simulated snow depth, sea ice thickness, and observed results were closest to each other.

3.3 *Sea ice growth and melting*

Sea ice growth included bottom growth, new ice formation, and snow ice formation, while reduction involved bottom and surface melting. In this study, the simulated sea ice surface remained continuously covered by snow, so surface melting primarily referred to the melting of the snow cover. The process of surface sublimation primarily affected the snow depth.

The contribution of bottom growth across different experiments is shown in Fig. 6. Compared to the Ctrl experiment, the Bulk and ITDrdg schemes demonstrated increased bottom growth as simulated snow depth decreased. Snow cover can insulate the heat exchange between sea ice and the atmosphere. A reduction in snow depth can lead to a decrease in sea ice temperature (Fig. 5), thereby increasing bottom growth. In the Ctrl experiment, bottom growth contributed 71.9 cm to sea ice growth. The maximum sea ice thicknesses in the seven simulated experiments were 148.4 cm, 150.7 cm, 152.2 cm, 153.6 cm, 154.5 cm, 156.6 cm, and 158.1 cm for Ctrl and Exps 1−6 experiments, respectively. After reaching maximum thickness, ice thickness decreased due to melting

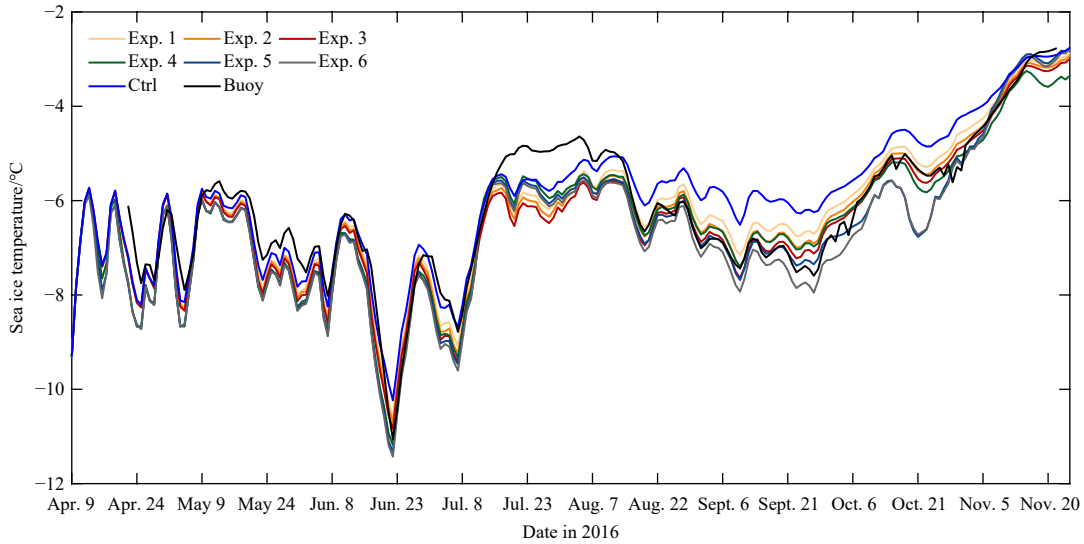


Fig. 5. Simulated sea ice temperature using different snow blowing parameterization scheme and observed sea ice temperature. Buoy means the temperature buoy observed sea ice temperature.

(Fig. 4). Before reaching maximum thickness, sea ice thickened by 71.7 cm, 73.9 cm, 75.5 cm, 76.9 cm, 77.7 cm, 79.9 cm, and 81.3 cm for Ctrl experiment and Exps 1−6 (Fig. 6), which included both bottom growth and snow ice formation, with bottom growth being the main contributor. Bottom growth in the Bulk and ITDrdg schemes increased by 3.8 cm, 5.3 cm, 6.6 cm, 5.4 cm, 7.8 cm, and 9.0 cm compared to the Ctrl experiment, with the maximum difference being 12.5% (9.0 cm in Exp. 6 compared to 71.7 cm in Ctrl).

The formation of snow ice decreased as simulated snow depth decreased (Fig. 7). In the Bulk scheme, only Exp. 2 had 0.3 cm of snow ice, while Exps 3 and 4 had almost none. In the ITDrdg scheme, snow ice depths were 2.7 cm, 2.6 cm, and 2.6 cm, smaller than the 3.0 cm in the Ctrl experiment. Compared to the average snow ice thick-

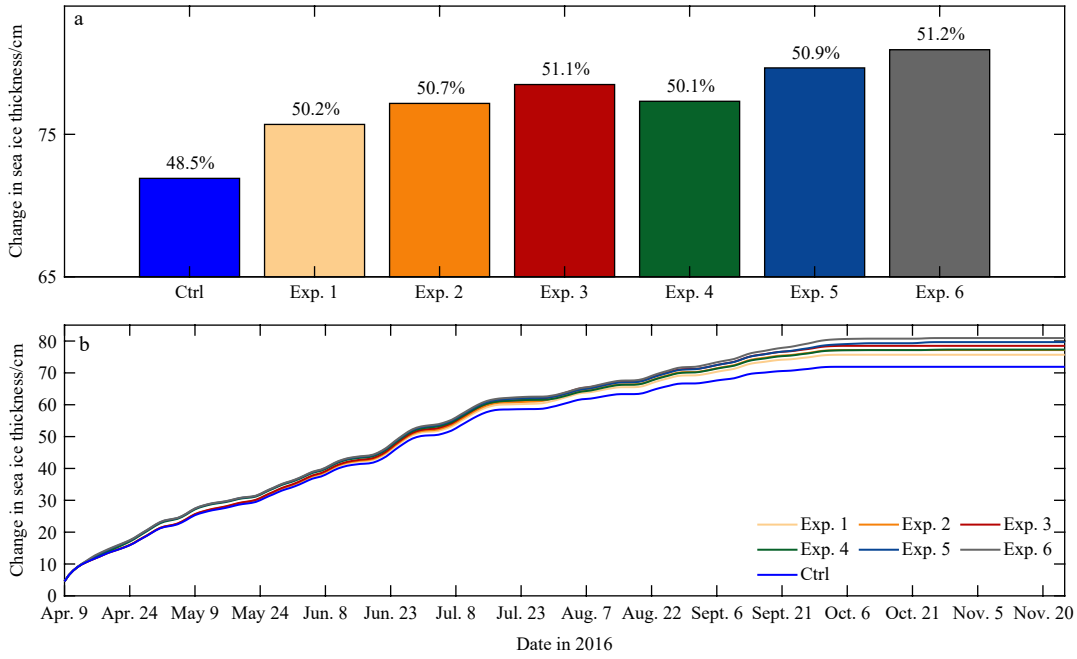


Fig. 6. Simulated sea ice congelation (a) and the accumulated sea ice congelation over time (b) using different snow blowing parameterization scheme, the percentage indicates the ratio of sea ice congelation to the maximum simulated sea ice thickness in each experiment, respectively.

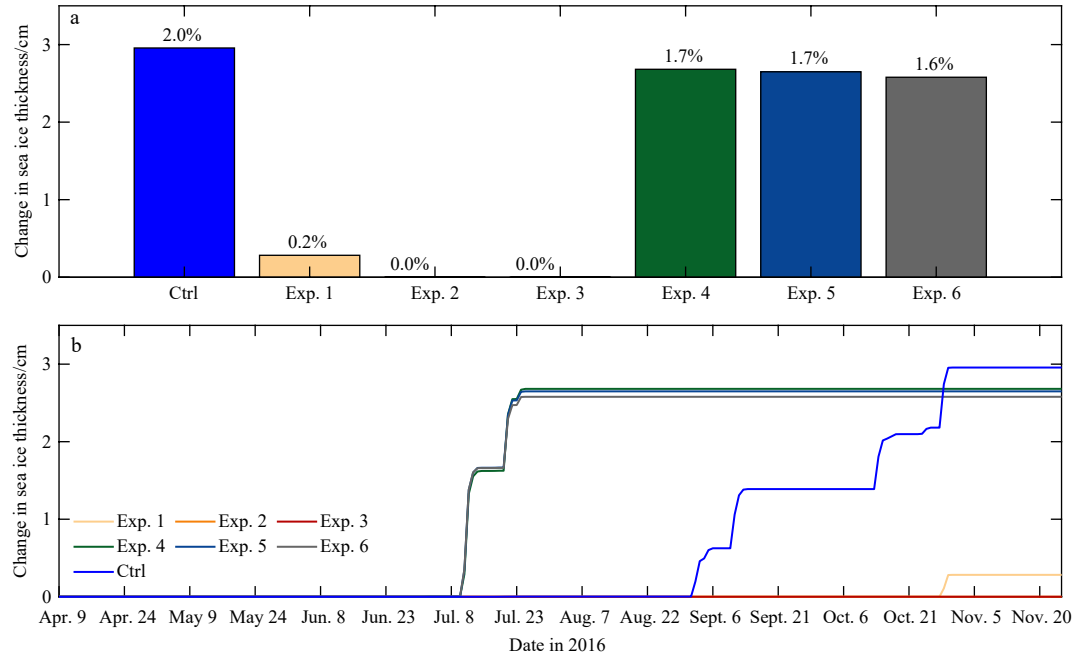


Fig. 7. Simulated snow ice (a) and the accumulated snow ice over time (b) using different snow blowing parameterization scheme, the percentage indicates the ratio of snow ice to the maximum simulated sea ice thickness in each experiment, respectively.

ness of 2.7 cm in other experiments, the Bulk scheme significantly reduced snow ice. Snow ice formed when thick snow cover caused negative freeboard thickness, leading to the replacement of snow with sea ice. In the ICEPACK simulations, snow ice formation depended on ice thickness, ice density, snow depth, and snow density. In the Ctrl experiment, snow ice formed primarily in the later stages, starting on September 1, with ice thickness and snow depth at 141.2 cm and 31.2 cm, respectively. In the ITDrdg scheme, snow ice formation mainly occurred on July 11, with ice thickness at 131.7 cm, 132.2 cm, and 132.5 cm, and snow depth at 23.2 cm, 22.7 cm, and 22.3 cm. In the Bulk scheme, snow ice formation occurred after October 29 in Exp. 1, with ice thickness and snow depth at 148.8 cm and 37.3 cm, respectively. The snow depth was larger than the results of the ITDrdg scheme when the snow ice began to form in Exp. 1. Reduced snowfall in the Bulk scheme resulted in almost no snow ice formation. In contrast, snow continued to accumulate in the Ctrl experiment, with snow ice forming mainly after September.

Sublimation differences among the simulated experiments were minimal with values of 8.1 cm, 7.9 cm, 7.8 cm, 7.6 cm, 7.7 cm, 8.0 cm, and 7.8 cm for the Ctrl experiment and Exps 1−6, respectively (Fig. 8). Snow sublimation occurred throughout the simulation period, increasing with air temperature after October. Snow surface melting began after November (Fig. 9) with temperature rising, at 3.2 cm in the Ctrl and Bulk experiments, and 2.7 cm, 2.2 cm, and 2.2 cm in the ITDrdg scheme experiments. Snow surface melting increased in the Bulk scheme. Bottom melting primarily occurred after October (Fig. 10), reaching 8.7 cm in the Ctrl experiment, with Bulk scheme showing maximum melting at 8.3 cm in Exp. 1. Bottom melting in the ITDrdg scheme experiments (Exps 5 and 6) exceeded Ctrl experiment results after middle November, at 9.7 cm and 9.2 cm, respectively.

3.4 *Influence of snow blowing*

Snow blowing primarily affects surface snow depth, which in turn influences sea ice growth through thermodynamic processes. In this study, the Ctrl experiment did not include snow blowing processes. In contrast, Exps 1−3 used the Bulk scheme to reduce snowfall reaching the ice surface, while Exps 4−6 employed the ITDrdg scheme to account for wind effects on snow, including snow transport and changes in snow density.

To illustrate the impact of snow blowing, we selected the Ctrl experiment, Exp. 3 (using the Bulk scheme), and Exp. 6 (using the ITDrdg scheme) for comparison over the period from September 14 to October 10, a period with no snowfall (Fig. 2c). On September 14, the snow depths in the Ctrl experiment, Exp. 3, and Exp. 6 were 38.5 cm, 30.1 cm, and 28.5 cm, respectively. The differences in snow depth were primarily due to the different snow blowing scheme used in these experiments. By October 10, the snow depths had decreased to 38.0 cm, 29.6 cm, and 24.7 cm, with reductions of 0.5 cm, 0.5 cm, and 3.8 cm, respectively. During this period, there was no surface melting or snow ice formation, so the decreases in snow depth were primarily attributed to sublimation and snow blowing. Both the Ctrl experiment and Exp. 3 experienced a 0.5 cm decrease in snow depth, while Exp. 6 saw a larger reduction of 3.8 cm due to snow blowing, ac-

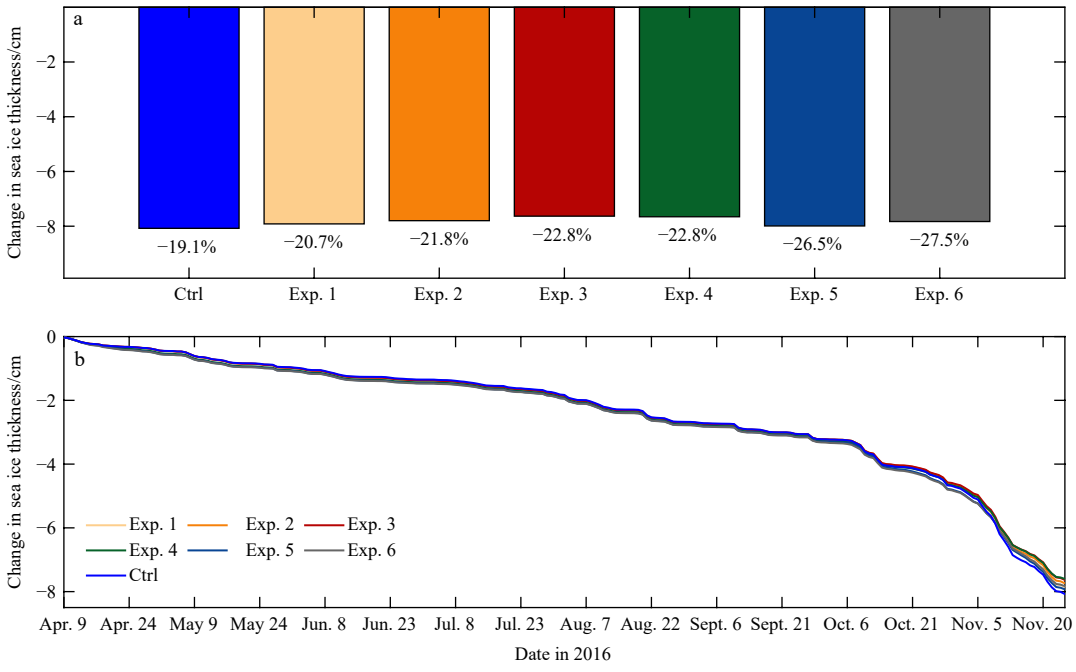


Fig. 8. Simulated snow sublimation (a) and the accumulated snow sublimation over time (b) using different snow blowing parameterization scheme, the percentage indicates the ratio of snow sublimation to the maximum simulated snow depth in each experiment, respectively.

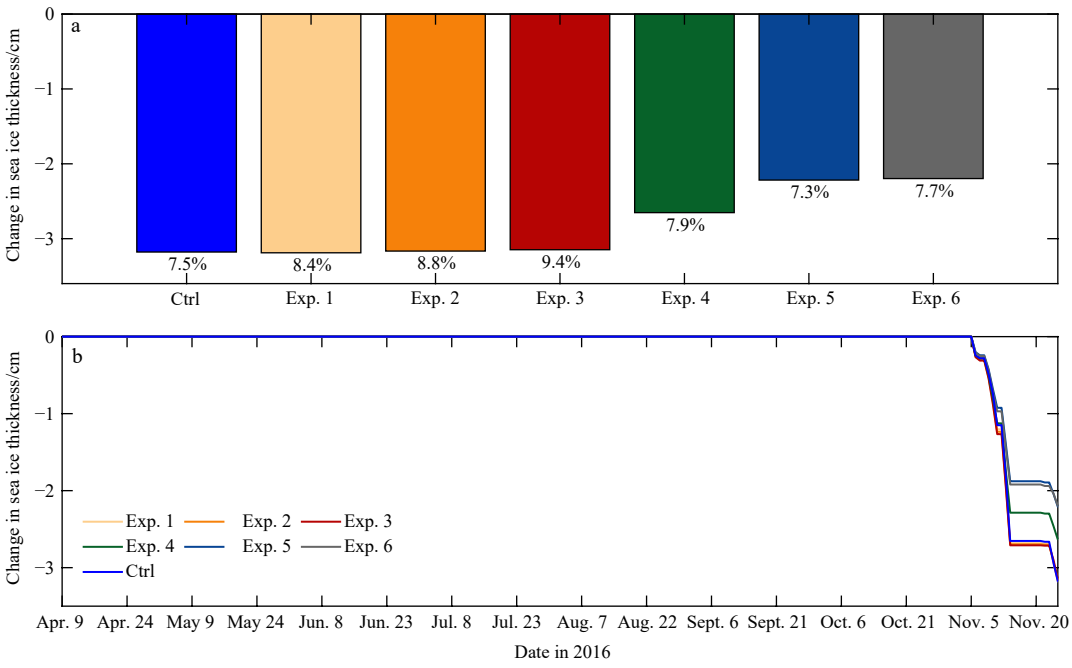


Fig. 9. Simulated snow melting (a) and the accumulated snow melting over time (b) using different snow blowing parameterization scheme, the percentage indicates the ratio of snow melting to the maximum simulated snow depth in each experiment, respectively.

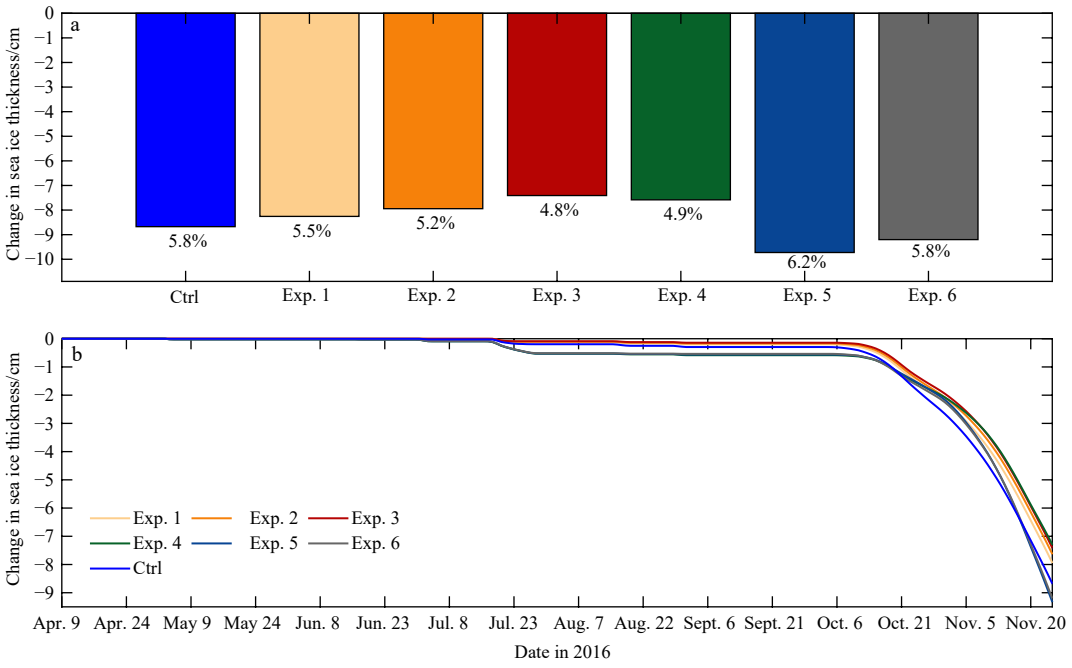


Fig. 10. Simulated sea ice bottom melting (a) and the accumulated sea ice bottom melting over time (b) using different snow blowing parameterization scheme, the percentage indicates the ratio of sea ice bottom melting to the maximum simulated sea ice thickness in each experiment, respectively.

counting for 11.6% of the initial snow depth (28.5 cm) on September 14. Cold temperatures during this stage indicate that snow blowing was the main factor reducing snow depth. Manual observations on September 13 and October 11, showing snow depths of 18.5 cm and 14 cm, respectively, closely matched the 4.5 cm shown reduction in Exp. 6.

Another period, from October 30 to November 26, was selected to examine the impact of snow blowing during a later stage, which included sublimation, melting, snowfall, and snow blowing processes. On October 30, the snow depths in the Ctrl experiment, Exp. 3, and Exp. 6 were 42.1 cm, 33.4 cm, and 27.5 cm, respectively. By November 26, these depths had decreased to 35.4 cm, 27.0 cm, and 15.2 cm, with reductions of 6.7 cm, 6.4 cm, and 12.3 cm, respectively. Although three snowfall events

occurred during this period, the increase in snow depth due to snowfall did not exceed 0.1 cm. Sublimation accounted for 3.4 cm, 3.0 cm, and 3.0 cm of snow reduction, while surface melting accounted for 3.2 cm, 3.1 cm, and 2.2 cm in the Ctrl experiment, Exp. 3, and Exp. 6, respectively. Therefore, compared to the Ctrl and Exp. 3 experiments, Exp. 6 exhibited an approximate 7.1 cm reduction in snow thickness due to snow blowing. During this stage, although sublimation and melting increased, snow blowing remained the primary process reducing snow depth. It is important to note that the simulation ended on November 26 and did not cover the entire melting season.

In summary, the snow blowing parameterization scheme used in ICEPACK improved the simulation of snow depth and sea ice thickness. The ITDrdg scheme aligned more closely with the physical processes of snow blowing, resulting in simulated snow depth and sea ice thickness that were in better agreement with *in situ* observations, particularly in capturing the trend of snow depth. However, due to the lack of *in situ* observations of snow blowing processes on the landfast sea ice near Zhongshan Station, our understanding of these processes remains limited.

4 Conclusions

The landfast sea ice thickness and snow depth were simulated and evaluated using the one-dimensional thermodynamic model ICEPACK based on observational data near Zhongshan Station from April to November 2016. This study focused on evaluating different snow blowing parameterization schemes and their impact on the simulation of snow depth and sea ice thickness. The simulated results were compared to buoy observations and manual observations of snow depth, sea ice thickness, and sea ice temperature. Furthermore, the study examined how various snow blowing parameterization schemes affected simulated snow accumulation, melt, and sea ice growth and melt processes in ICEPACK. A total of seven experiments were conducted, including a Ctrl experiment without a snow blowing scheme, three experiments using the Bulk scheme, and three using the ITDrdg scheme. The simulations primarily focused on the sea ice growth period, including the early stages of melting.

The simulation results indicated that snow depth simulations using the snow blowing scheme closely matched the observations, as evidenced by root mean square errors (RMSEs) of less than 10 cm for the ITDrdg scheme. As snow depth simulations improved, the sea ice thickness simulation also became more consistent with the observed results, with RMSEs for sea ice thickness less than 10 cm using the ITDrdg scheme. In contrast, the Ctrl experiment, which lacked a snow blowing scheme, yielded the thickest snow depth, thinnest ice thickness, and the largest error compared to observations, with RMSE of 12.5 cm and 14.9 cm for snow depth and sea ice thickness, respectively. The thicker simulated snow depth in the Ctrl experiment led to higher simulated sea ice temperatures, with an RMSE of 0.7℃. Among all experiments, Exp. 6 using the ITDrdg scheme exhibited the smallest average error and RMSE compared to observations. However, the simulated sea ice temperatures using the snow blowing scheme were generally lower than the observed sea ice temperatures. Exp. 6 had the largest error in simulating sea ice temperature compared to the observed results, while Exp. 1 had the smallest error.

Snow undergoes various processes, including sublimation, melting, and snow ice transformation. Snow blowing process mainly affected snow depth, which in turn influenced sea ice thermodynamic growth. Changes in snow depth primarily affect the bottom growth of sea ice, the most important part of sea ice growth. The simulations showed little differences in snow sublimation, slight differences in snow melting and sea ice bottom melting, and the largest differences in sea ice bottom growth due to influence of snow depth. The simulated sea ice thickness increased by 71.7 cm, 73.9 cm, 75.5 cm, 76.9 cm, 77.7 cm, 79.9 cm, and 81.3 cm for the Ctrl and Exps 1−6 experiments, respectively, primarily due to bottom growth with little snow ice formation. The Ctrl experiment had the most snow ice formation throughout the simulation period, with 3.0 cm. The simulated sea ice thickness using the Bulk and ITDrdg schemes showed increased bottom growth of 3.8 cm, 5.3 cm, 6.6 cm, 5.4 cm, 7.8 cm, and 9.0 cm compared to the Ctrl experiment, respectively. Notably, Exp. 6 showed a 12.5% increase in bottom growth compared to Ctrl.

Simulations using the snow blowing scheme effectively reduced snow accumulation. Both the simulated snow depth using the Bulk and ITDrdg schemes were smaller than the Ctrl experiment. While the Bulk scheme did not consider snow blowing effects after snowfall reached the ice surface, the ITDrdg scheme continued to account for wind effects on snow. Snow blowing was the main factor influencing snow depth changes after snowfall, showing a more significant impact on snow depth reduction than sublimation, snow ice formation, and surface melting. The simulation results using the ITDrdg snow blowing parameterization scheme were more reasonable when compared to observations.

Snow blowing processes, often influenced by katabatic winds, are common in Antarctica, particularly on landfast sea ice near Zhongshan Station. Snow blowing is an important factor affecting changes in snow depth. However, observing and studying snow blowing remains challenging due to a lack of *in situ* observations. Future work should focus on long-term *in situ* observations, data collection, and analysis of snow blowing characteristics, as well as verification and evaluation of snow blowing parameterization schemes to enhance simulation results.

Acknowledgements

We show our great appreciation to the wintering team of the 32nd CHINARE for the field observations supporting. We also thank the Chinese Arctic and Antarctic Administration and Polar Research Institute of China for the logistic support.

References

Cheng Bin, Launianen J, Vihma T. 2003. Modelling of superimposed ice formation and subsurface melting in the Baltic Sea. Geophysica, 39(1): 31–50

Collins W D, Bitz C M, Blackmon M L, et al. 2006. The community climate system model version 3 (CCSM3). Journal of Climate, 19(11): 2122–2143, doi: 10.1175/JCLI 3761.1

Durand Y, Guyomarc'h G, Mérindol L, et al. 2005. Improvement of a numerical snow drift model and field validation. Cold Regions Science and Technology, 43(1/2): 93–103, doi: 10.1016/j.coldregions.2005.05.008

Hao Guanghua, Pirazzini R, Yang Qinghua, et al. 2021a. Spectral albedo of coastal landfast sea ice in Prydz Bay, Antarctica. Journal of Glaciology, 67(261): 126–136, doi: 10.1017/jog.2020.90

Hao Guanghua, Shen Hui, Sun Yongming, et al. 2021b. Rapid decrease in Antarctic sea ice in recent years. Acta Oceanologica Sinica, 40(7): 119–128, doi: 10.1007/s13131-021-1762-x

Hao Guanghua, Yang Qinghua, Zhao Jiechen, et al. 2019. Observation and analysis of landfast ice arounding Zhongshan Station, Antarctic in 2016. Haiyang Xuebao (in Chinese), 41(9): 26–39, doi: 10.3969/j.issn.0253-4193.2019.09.003

Hobbs W R, Massom R, Stammerjohn S, et al. 2016. A review of recent changes in Southern Ocean sea ice, their drivers and forcings. Global and Planetary Change, 143: 228–250, doi: 10.1016/j.gloplacha.2016.06.008

Hunke E, Allard R, Bailey D A, et al. 2021. CICE-consortium/icepack: icepack 1.3. 0. https://github.com/CICE-Consortium/Icepack/wiki/Icepack-Release-Table [2021-09-03], doi: 10.5281/zenodo.5423061

Kwok R, Kacimi S. 2018. Three years of sea ice freeboard, snow depth, and ice thickness of the Weddell Sea from operation IceBridge and CryoSat-2. The Cryosphere, 12(8): 2789–2801, doi: 10.5194/tc-12-2789-2018

Lecomte O, Fichefet T, Flocco D, et al. 2015. Interactions between wind-blown snow redistribution and melt ponds in a coupled ocean–sea ice model. Ocean Modelling, 87: 67–80, doi: 10.1016/j.ocemod.2014.12.003

Leppäranta M. 1983. A growth model for black ice, snow ice and snow thickness in subarctic basins. Hydrology Research, 14(2): 59–70, doi: 10.2166/nh.1983.0006

Lewis M J, Tison J L, Weissling B, et al. 2011. Sea ice and snow cover characteristics during the winter-spring transition in the Bellingshausen Sea: an overview of SIMBA 2007. Deep Sea Research Part Ⅱ: Topical Studies in Oceanography, 58(9–10): 1019–1038, doi: 10.1016/j.dsr2.2010.10.027

Mott R, Schirmer M, Bavay M, et al. 2010. Understanding snow-transport processes shaping the mountain snow-cover. The Cryosphere, 4(4): 545–559, doi: 10.5194/tc-4-545-2010

Parkinson C L. 2019. A 40-y record reveals gradual Antarctic sea ice increases followed by decreases at rates far exceeding the rates seen in the Arctic. Proceedings of the National Academy of Sciences of the United States of America, 116(29): 14414–14423, doi: 10.1073/pnas.1906556116

Powell D C, Markus T, Stössel A. 2005. Effects of snow depth forcing on Southern Ocean sea ice simulations. Journal of Geophysical Research: Oceans, 110(C6): C06001, doi: 10.1029/2003JC002212

Sturm M, Holmgren J, Perovich D K. 2002. Winter snow cover on the sea ice of the Arctic Ocean at the surface heat budget of the Arctic Ocean (SHEBA): temporal evolution and spatial variability. Journal of Geophysical Research: Oceans, 107(C10): 8047, doi: 10.1029/2000JC000400

Sun Qizhen, Zhang Lin, Zhang Zhanhai, et al. 2016. Numerical simulation of summer katabatic wind at Zhongshan Station, Antarctica: a case study. Haiyang Xuebao (in Chinese), 38(3): 71–81, doi: 10.3969/j.issn.0253-4193.2016.03.007

Trujillo E, Leonard K, Maksym T, et al. 2016. Changes in snow distribution and surface topography following a snowstorm on Antarctic Sea ice. Journal of Geophysical Research: Earth Surface, 121(11): 2172–2191, doi: 10.1002/2016JF003893

Vionnet V, Martin E, Masson V, et al. 2014. Simulation of wind-induced snow transport and sublimation in alpine terrain using a fully coupled snowpack/atmosphere model. The Cryosphere, 8(2): 395–415, doi: 10.5194/tc-8-395-2014

Wang Caixin, Cheng Bin, Wang Keguang, et al. 2015. Modelling snow ice and superimposed ice on landfast sea ice in Kongsfjorden, Svalbard. Polar Research, 34(1): 20828, doi: 10.3402/polar.v34.20828

Willatt R C, Giles K A, Laxon S W, et al. 2010. Field investigations of Ku-band radar penetration into snow cover on Antarctic sea ice. IEEE Transactions on Geoscience and Remote Sensing, 48(1): 365–372, doi: 10.1109/TGRS.2009.2028237

Xie Simei, Mei Shan, Liu Kewei, et al. 2002. Cyclone formation and development in the Antarctic Prydz Bay. Acta Oceanologica Sinica, 21(1): 45–54

Zuo Hao, Balmaseda M A, Tietsche S, et al. 2019. The ECMWF operational ensemble reanalysis-analysis system for ocean and sea ice: a description of the system and assessment. Ocean Science, 15(3): 779–808, doi: 10.5194/os-15-779-2019